Construction and calibration of an instrument for three-dimensional ion imaging

Konrad Koszinowski, Noah T. Goldberg, Andrew E. Pomerantz,[a] and Richard N. Zare[b]
Department of Chemistry, Stanford University, Stanford, California 94305-5080

(Received 6 April 2006; accepted 31 May 2006; published online 4 October 2006)

We describe a new instrument based on a delay-line detector for imaging the complete three-dimensional velocity distribution of photoionized products from photoinitiated reactions. Doppler-free [2+1] resonantly enhanced multiphoton ionization (REMPI) of H and D atoms formed upon photolysis of HBr and DBr in the range 203 nm$\leqslant\lambda_{\text{photolysis}}\leqslant$243 nm yields radial speeds measured to be accurate within 1% of those calculated. The relative speed resolution is about 5% and limited by photoionization recoil broadening. A relative speed resolution of 3.4% is obtained for [3+1] REMPI, which minimizes the ionization recoil. We also determine the branching ratio between ground-state and spin-orbit-excited product channels and their associated anisotropies. We find that DBr photolysis dynamics differs slightly from its HBr counterpart. © *2006 American Institute of Physics*. [DOI: 10.1063/1.2217742]

I. INTRODUCTION

The scattering angle is a sensitive probe for the detailed mechanism of a bimolecular reaction.[1] Therefore, its determination, i.e., the recording of differential cross sections, remains a central goal in reaction dynamics. One approach toward this aim relies on the method of crossed molecular beams pioneered by Lee and Herschbach.[2–4] While highly successful in general, this technique can have some blind spots in the angular distribution caused by blocking of the detector by the beam sources or by interference from one the reactant beams.

An alternative approach that, in favorable cases, can overcome this limitation is given by the so-called PHOTOLOC technique (photoinitiated reaction analyzed by the law of cosines).[5,6] This method uses only a single molecular beam containing one reactant and a precursor that yields the second reactant upon photolysis. If the energetics and kinematics of the system are known and a monochromatic light source (typically a laser) is applied, the speed of the center of mass $u_{\text{c.m.}}$ and the center-of-mass speed of a particular product u_{prod} are easily calculated. However, the orientation of the product's trajectories and thus the scattering angle θ are undetermined unless v_{prod}, the speed of the product in the laboratory frame and the third side of the triangle spanned by $u_{\text{c.m.}}$ and u_{prod}, is known (Fig. 1). Thus, the problem of measuring angular distributions is transformed into the determination of speed distributions.

It is important to note that the velocity distributions in PHOTOLOC experiments are necessarily three-dimensional (3D) because, unlike the crossed-beam technique, the orientation of the center-of-mass velocity $u_{\text{c.m.}}$ is not fully controlled, and averaging over all angles occurs. If only a one-dimensional (1D) detector is used, it has to be ensured that no products with significant off-axis velocity contributions are collected because, otherwise, the measured speed would not correspond to v_{prod}. This task can be achieved simply by placing a conical mask in front of the detector. While this so-called core-extraction technique has been successfully applied to several different reactive systems,[7,8] it has the obvious drawback of sacrificing most of the signal's intensity. This downside is particularly detrimental to the study of reactions with low cross sections. In addition, the sensitivity of core extraction depends on the scattering angle and is lowest for forward scattering, thus somewhat limiting its potential advantage over crossed-beam techniques.

A different approach involves the two-dimensional (2D) projection of the photoionized product's velocity distribution onto a position-sensitive detector.[9,10] In conventional ion imaging, the temporal information is lost because the response of the detector (usually a combination of microchannel plates, phosphor screen, and charge-coupled device camera) is too slow. To reconstruct the 3D velocity distributions from the 2D images, numerical inversion techniques must be applied. This procedure can introduce artifacts unless a more sophisticated analysis is applied.[11–14] Recent improvements have centered on delaying the extraction of the photoionized products and thereby spreading their arrival times at the detector. Fast gating of the detector then directly yields the central time slice of the 3D product velocity distribution.[15–18]

Delayed extraction and gating are not necessary if an inherently fast detector is used. Such a device may be realized by coupling a microchannel-plate (MCP) stack to a delay-line anode, a special arrangement of pairs of wires held at different electrical potentials.[19] Each arriving ion triggers a laterally confined electron avalanche within the MCPs and the emission of a pulse of electrons from the back of the MCP stack. The electrons are accelerated toward the delay-line anode, where they induce an electric signal traveling to both ends of each pair of wires. The lateral position can be determined from the difference of arrival times at the two

[a]Present address: Schlumberger-Doll Research, 36 Old Quarry Rd., Ridgefield, CT 06877.
[b]Electronic mail: zare@stanford.edu

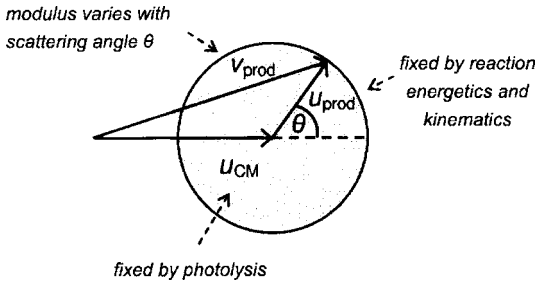

FIG. 1. Collapsed Newton diagram illustrating the PHOTOLOC technique. Measurement of the laboratory product speed $|v_{prod}|$ uniquely determines the triangle spanned by the center-of-mass velocity $u_{c.m.}$ and the center-of-mass product velocity u_{prod}, and thus permits straightforward calculation of the center-of-mass scattering angle θ from the law of cosines.

opposite ends of a given pair of wires, and the time sum serves as a measure for the absolute arrival time and thus provides information on the third dimension. Delay-line anodes were originally developed for studying atom ionization at high energies,[20] but have also been successfully used for the investigation of unimolecular reactions, such as photodissociation and dissociative photoionization.[21–25] This type of detector appears equally well suited for the measurement of speed distributions in bimolecular reactions and the determination of differential cross sections according to the PHOTOLOC technique.

In the present contribution, we report the construction and calibration of a new 3D ion-imaging instrument based on the combination of a delay-line detector and a Doppler-free photoionization scheme, which is able to achieve a relative speed resolution of a few percent. We focus on the photodissociation of HBr and DBr as test systems because the photolysis of the former has been studied extensively and is well understood.[26–29] In addition, HBr photolysis provides fast hydrogen atoms, which can be employed as reactants in the $H+D_2$ exchange reaction. We plan to use the new instrument for the detailed investigation of the dynamics of this pivotally important reaction.

II. EXPERIMENTAL APPARATUS

The apparatus comprises a vacuum chamber equipped with a nozzle valve for reagents inlet and windows for the entrance of the photolysis and photoionization laser light. The vacuum chamber also houses a time-of-flight mass spectrometer and the detector.

A. Vacuum chamber and reagents inlet

The vacuum chamber consists of a stainless steel tube pumped by two turbomolecular pumps (Varian TV 1001 Navigator), whose exhaust passes a liquid nitrogen cooled trap, and a filter element for trapping residual HBr/DBr before it is fed into a dry scroll pump (Varian Triscroll 600). This setup completely eliminates the use of pump oil and excludes possible contaminations caused by backstreaming. All pumps are continuously purged with dry nitrogen to minimize corrosion by HBr/DBr. Typical pressures in the detection region as measured by a Bayard-Alpert ionization gauge are 4×10^{-9} mbar without and 2×10^{-7} mbar with the nozzle operational.

Reagents are introduced through a pulsed nozzle valve (General Valve Corporation, series 900 pulsed solenoid valve, cylindrical body, 0.8 mm orifice, Kel-F poppet). The nozzle can be aligned by an *xyz* vacuum manipulator while it is conveniently viewed through a window. An Iota One (General Valve Corporation) pulse driver produces gas pulses, which last ~300 μs and expand vertically downward (*z* direction). For the photodissociation experiments, HBr (Matheson, research grade) or DBr (Cambridge Isotope Laboratories, 99% D) were purified by a freeze-pump-thaw cycle before 20-fold dilution in Ar (Liquid Carbonic, 99.998%). Mixtures of 1000–1500 mbar stagnation pressure were prepared and kept in a glass manifold protected from light and fed into the nozzle via a Teflon line.

The vacuum chamber contains ports for the laser beams in the horizontal (*xy*) plane perpendicular to the molecular beam. These ports are directly sealed by fused silica windows or first attached to nipples with optical baffles to minimize stray light (see Sec. III C).

B. Optical system

For HBr and DBr photolysis between 203 and 233 nm, pulses of vertically polarized light (≤6 mJ/pulse, 5 ns width, 10 Hz) are generated by frequency tripling the output of a dye laser (Quanta-Ray PDL-1) pumped by the second harmonic of a Nd:YAG (yttrium aluminum garnet) laser (Quanta-Ray DCR-3). The tripled light is separated from the fundamental and second harmonic by dichroic mirrors and focused onto the molecular beam by a 600 mm fused silica positive lens. Accurate calibration of the dye laser was achieved by measuring the [2+1] resonantly enhanced multiphoton ionization (REMPI) spectra for the *Q* branch of the $E,F\,^1\Sigma_g^+ - X\,^1\Sigma_g^+$ (0,0) band of H_2 at $\lambda\approx201.7$ nm (Ref. 30) and for the $2s(^2S_{1/2}) \leftarrow 1s(^2S_{1/2})$ transition of atomic H at $\lambda=243.1$ nm.[31]

For the detection of the H or D atoms formed upon photolysis of HBr and DBr, respectively, [2+1] REMPI via the $2s(^2S_{1/2}) \leftarrow 1s(^2S_{1/2})$ transition is used again. 243 nm light (≤4 mJ/pulse) is obtained by frequency doubling the output of a dye laser (Lambda Physik LPD 3000) pumped by the third harmonic of a Nd:YAG laser (Quanta-Ray DCR-1). The doubled light is separated by dichroic mirrors, expanded by a 1:3 Galilean telescope, and tightly focused onto the molecular beam by a 350 mm fused silica lens. The power of the light can be attenuated in a controlled way by tilting its polarization axis with a half-wave plate and filtering out the horizontal component with a polarizer. The same setup is used for generating light of $\lambda\approx251$ nm, which is needed to record [2+1] REMPI spectra of the *Q* branch of the $H\,^1\Sigma^+ - X\,^1\Sigma^+$ (0,0) band of HBr.[32] For Doppler-free spectroscopy (see Sec. IV B), the light is divided by a 50:50 beam splitter and enters the vacuum chamber in a counterpropagating geometry (perpendicular to the photolysis beam).

In addition, H atoms are detected by [3+1] REMPI via the $2p(^2P_{3/2}) \leftarrow 1s(^2S_{1/2})$ transition.[33] Up to 8 mJ/pulse of the

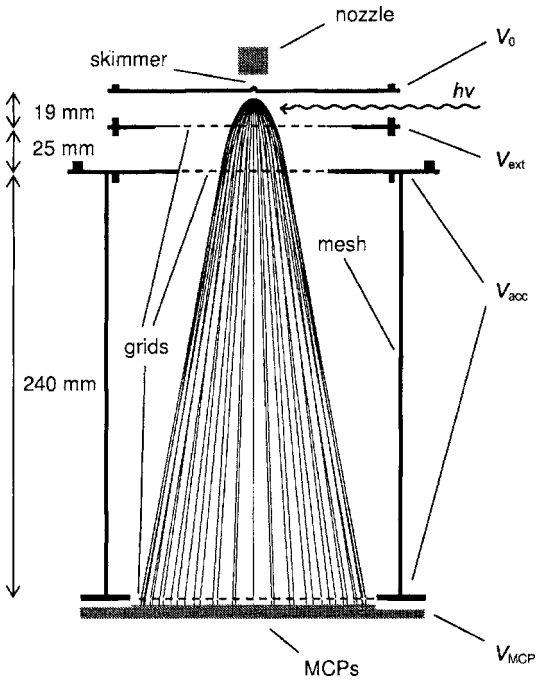

FIG. 2. Profile of the TOF mass spectrometer and ion trajectories predicted by SIMION calculations. The path of the incident laser light is indicated.

required 364.7 nm light (vertically polarized) is obtained by frequency mixing the output of a dye laser (Lambda Physik LPD 3000) pumped by the second harmonic of a Nd:YAG laser (Quanta-Ray GCR-4) with the IR fundamental of the latter. The 364.7 nm light is separated by dichroic mirrors, expanded by a 1:3 Galilean telescope, and tightly focused onto the molecular beam by a 150 mm lens. For the ionization of H_2, HD, and D_2 needed for the calibration of the time-of-flight mass spectrometer (Sec. III B), [2+1] REMPI is employed as described above.

C. Time-of-flight mass spectrometer

The laser beams intersect the molecular beam in the ionization region of a homebuilt time-of-flight (TOF) mass spectrometer. The molecular beam enters through a conical skimmer (1.0 mm orifice) directly attached to the center of the first electrode (Fig. 2). Typically, the nozzle valve is lowered to a distance of ~5 mm from the top of the skimmer, which in turn protrudes by 2 mm over the first electrode. While Chichinin *et al.*[22] place their TOF mass spectrometer perpendicular to the molecular beam in their delay-line instrument, we choose a collinear orientation. This arrangement ensures effective electric shielding of the mass spectrometer by the first electrode without the need for additional guard electrodes. To avoid electric discharge from the edge of the skimmer, the first electrode is grounded (V_0=0) such that no potential difference exists with respect to the nozzle. Note that the laser beams do not intersect the molecular beam in the center between the first and second electrodes, but more closely to the former. This configuration allows us to achieve higher signal intensities if necessary while maintaining good resolution and space focusing (see Sec. III B).[34] Increased signal intensities should be especially beneficial for the investigation of bimolecular reactions, which have inherently lower signal levels than photodissociation processes.

Application of a negative potential to the second electrode (V_{ext}) creates a homogeneous electric field, which extracts the positive ions formed upon photoionization into the second region of the mass spectrometer. Here, the ions are further accelerated until they pass the third electrode (held at V_{acc}) and enter the field-free drift region. The entire field-free region is shielded by wire mesh to protect it from perturbation by stray electric fields without compromising the pumping characteristics. This measure proves effective for achieving a high vacuum in the detection region without differential pumping (see Sec. II A). We are not aware of a similar design described in the literature. After leaving the drift region, the ions are accelerated to the front face of the MCP stack.

The electrodes are made of stainless steel and held together by ceramic rods with a 1 GΩ resistive coating (Macro Metals, San Jose, CA). This coating is intended to prevent the build up of charge without allowing a significant current flow between the electrodes. To minimize electric field leakage from one compartment to the other, these are separated by electroformed grids (3.5 lines/mm; Thin Metal Parts, Colorado Springs, CO) spot-welded to the second and third electrodes as well as to the end cap of the TOF mass spectrometer (Fig. 2).

A homebuilt voltage divider is used to apply V_{ext} and V_{acc} to electrodes 2 and 3. Typical voltages range from −10 to 1500 V, with relative precisions better than 0.1%. SIMION simulations confirmed that ion trajectories under normal operation conditions should not show appreciable deviations from ideal behavior (Fig. 2).[35]

D. Detector

The detector consists of a pair of 120 mm active diameter MCPs mounted in a Chevron configuration and a delay-line anode DLD120 with a time-to-digital converter (Roent-Dek, Kelkheim, Germany). Under typical operation, the front MCP is held at −2300 V and the second MCP is grounded. The signal and reference wires of the delay line are at +510 and +470 V, respectively, and the anode holder is at +150 V. For both x and y directions, one pair of signal/reference wires provides one differential signal (arrival time) for each end: $\tau(x_1)$, $\tau(x_2)$, $\tau(y_1)$, and $\tau(y_2)$. The lateral position (x,y) of the detected event can then be recovered from

$$x = s_x \cdot [\tau(x_1) - \tau(x_2)] = s_x \cdot \Delta\tau_x \tag{1a}$$

and

$$y = s_y \cdot [\tau(y_1) - \tau(y_2)] = s_y \cdot \Delta\tau_y, \tag{1b}$$

where s_x and s_y are the effective speeds of signal propagation in x and y directions, respectively. Because the wires are helically wound, the effective signal propagation perpendicular to the winding is much slower than the actual propagation of electric fields. The geometrical arrangement of the delay line causes the effective signal speeds to vary slightly for each dimension and this variation must be determined in the

calibration process ($s_x \approx s_y \approx 0.80$ mm/ns). The absolute time of the detected event τ is reconstructed by simple summation,

$$\tau = \tau(x_1) + \tau(x_2) + \tau_{\text{ref}} = \tau(y_1) + \tau(y_2) + \tau_{\text{ref}}, \quad (2)$$

where τ_{ref} is an absolute reference time. The equality in Eq. (2) within experimental uncertainty serves as a criterion to distinguish real events from artifacts.

The differential anode signals as well as the signal from the MCP stack are amplified to amplitudes of ~300 mV. A discriminator rejects electronic noise with adjustable thresholds between 15 and 100 mV. The amplified signals are then fed into a time-to-digital converter (TDC), whose output is read by a personal computer (PC). In addition, one of the amplified signals is sent to a digital oscilloscope (Tektronix TDS620). Visualization on the oscilloscope is particularly helpful for signal optimization.

E. Data acquisition

Four digital delay generators (Stanford Research Systems DG535) provide triggers at 10 Hz to control the timing of the photolysis and probe lasers, the nozzle pulse driver, the oscilloscope, and the TDC. The time settings, in particular, the firing of the lasers, can be varied during an experiment by LABVIEW (National Instruments, version 7.0) routines.

For data acquisition with the delay-line detector, we use a modified version of the COBOLDPC software package (RoentDek, Kelkheim, Germany), which can read an extra sync channel for communication with the other automated components of the experiment. The program allows us to set a time window for signal detection and to record species of only a single m/z ratio such as H^+ or D^+. The position and time lists of the detected events are then analyzed with the MATLAB program suite (version 7.0.1).

III. INSTRUMENT CHARACTERIZATION

A. Molecular beam

An important function of the nozzle valve is to cool the reagents introduced into the vacuum chamber by supersonic expansion. Cooling of photolytic precursors such as HBr and DBr is desirable because it narrows their internal energy distributions that otherwise will significantly broaden the speed distributions of their photofragments. Whereas vibrational excitation of HBr and DBr is negligible due to the large energy spacing between $v=0$ and $v=1$, rotational excitation must be considered. We therefore measured the rotational distribution of HBr in the molecular beam by [2+1] REMPI. The cooling varies strongly within the time profile of the gas pulse; the best cooling was achieved at the maximum of the pulse intensity, close to its rising flank. Other factors, such as opening time of the nozzle and its distance from the skimmer, the poppet material, and the stagnation pressure proved to be less important and could be varied over a wide range without significantly compromising the performance of the nozzle. Typically, the rotational distributions recorded could not be described by a single temperature; rather, the higher rotational states showed more population relative to thermodynamic equilibrium (Fig. 3). For the coolest distribution measured, a rotational temperature $T_{\text{rot}} \approx 40$ K can be assigned to $J=0-2$, whereas $T_{\text{rot}} \geqslant 120$ K is found for the higher rotational states. This distribution corresponds to an averaged rotational energy of $E_{\text{rot}}=0.007$ eV. More typically, $E_{\text{rot}}=0.016$ eV was obtained. These amounts of internal energy must be taken into account for calculating the speeds of the photofragments.

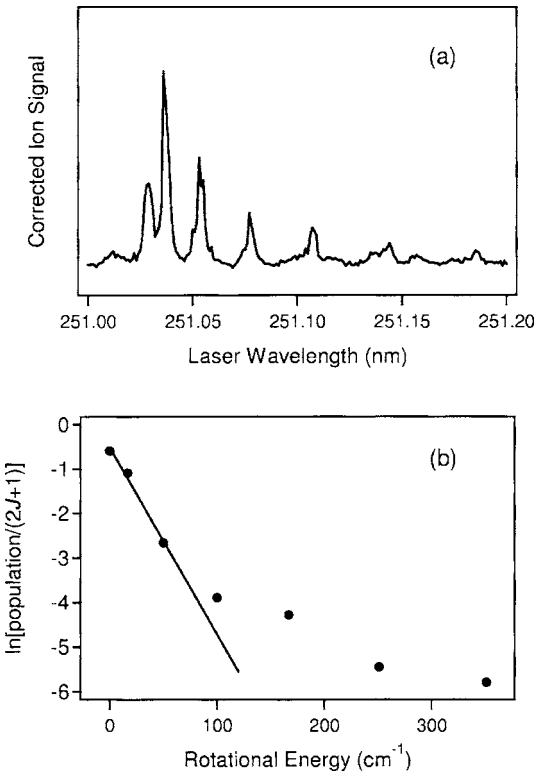

FIG. 3. (a) [2+1] REMPI spectrum of jet-cooled HBr and (b) Boltzmann plot of the corresponding rotational distribution. A rotational temperature $T_{\text{rot}} \approx 40$ K can be assigned to $J=0$-2 (straight line), but does not properly describe the population of the higher rotational states.

B. Time-of-flight mass spectrometer

In the present experiment the TOF mass spectrometer is not primarily used as an analytical tool, but rather as a device for the controlled acceleration of ions toward the detector. Our goal is the precise determination of the velocity of the neutral atoms or molecules *before* their ionization. While conservation of the velocity components in the x and y directions is trivial in the absence of electric fields in the xy plane, the situation is more complicated for the velocity component in the z direction, v_z. We would like to operate the mass spectrometer in such a way that the measured differences in the flight times of the ions $\Delta\tau$ are directly proportional to the different speed components v_z of the corresponding neutrals ($\Delta\tau$ is relative to the zero-velocity flight time, neutrals moving toward the detector should yield ions that arrive at the detector earlier than those that stem from neutrals originally moving away from it):

$$\nu_z = c_z \cdot \Delta\tau. \quad (3)$$

This condition is met when the mass spectrometer is operated in the Wiley-McLaren space-focusing configuration.[34] In this configuration, the flight time of an ion does not depend on the position of ionization to first order, which ensures the required proportionality between flight time and ν_z, as given by Eq. (3). This position independence has the additional advantage that even a relatively large ionization volume hardly blurs the measured speed distribution in the z direction.

For the given geometry (Fig. 2), space focusing is predicted for a voltage ratio of $V_{acc}/V_{ext}=3.97$.[34] This prediction assumes an ideal Wiley-McLaren configuration and neglects the additional path the ions must travel from the end of the field-free region to the MCPs. The effective drift region is therefore slightly longer than assumed in the calculation, which means that the predicted value for V_{acc}/V_{ext} should be too low. Experimental determination of space-focusing conditions for H_2, HD, and D_2 for different sets of voltages indeed yielded a slightly higher ratio $V_{acc}/V_{ext}=3.99$ on average.

Although our main objective is the determination of relative rather than absolute flight times, we briefly studied the latter as functions of m/z ratio (H_2^+ vs HD^+ vs D_2^+) and voltage ($-300\ \text{V} \leqslant V_{ext} \leqslant -16\ \text{V}$, $V_{acc}=3.99V_{ext}$) as well. For the prediction of absolute flight times, we varied the dimensions of the TOF mass spectrometer in our simulation within the uncertainties of measurement until the best overall agreement with the experimentally determined flight times was achieved. While the relative deviations between prediction and experiment were equal to or smaller than 0.3% for $V_{ext} \geqslant -35$ V, they increased up to 0.6% for $V_{ext}=-16$ V. This behavior possibly indicates the presence of stray weak electric fields whose effect is strongest for low voltages V_{ext} and V_{acc}. Rough measurements and calculations show that the influences of magnetic and gravitational fields are negligible.

C. Detector

Although the laser beams should not hit any reflective surface on their paths through the ionization region of the TOF mass spectrometer, stray UV light produced strong signals on the detector. Initially, these signals were so large that even at moderate laser powers (<1 mJ/pulse) we could not operate the front MCP at its normal voltage of $V_{MCP}=-2300$ V without the risk of damaging the detector (exponential gain curve for $-1600\ \text{V} \geqslant V_{MCP} \geqslant -2300\ \text{V}$). Apparently, the large size of the detector makes it particularly sensitive to stray UV light; Chichinin *et al.*,[22] who use an analogous 80 mm diameter detector, do not report similarly serious problems. By mounting the windows at Brewster's angle and using blackened nipples as well as optical baffles, we reduced the stray light to an acceptable level. These efforts were only required for light in the deep UV, whereas 365 nm radiation did not cause any response of the detector.

Obtained ion images display spherical shapes (Fig. 4), which rules out artificial distortions in the imaging. Moreover, it has been demonstrated that the type of MCPs employed has constant detection efficiency over its entire area.[36] The smooth intensity distributions in the recorded images are another indication of proper operation. If the thresholds for the discriminator are poorly adjusted, the detection efficiency becomes inhomogeneous and different numbers of events are recorded for the x and y dimensions.

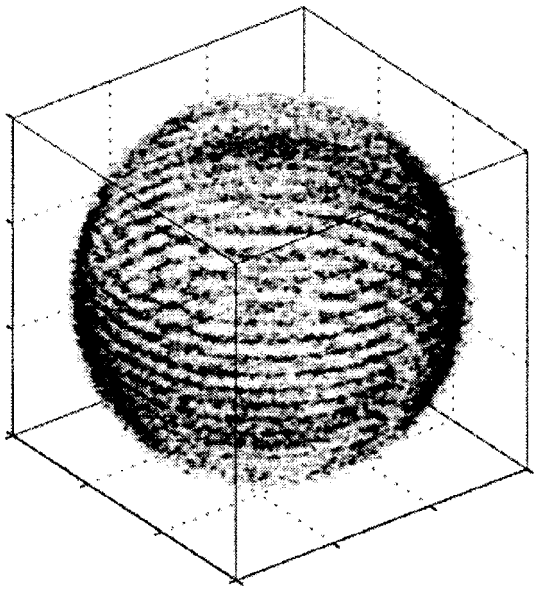

FIG. 4. Slices of the measured (unsymmetrized) 3D velocity distribution of H atoms formed upon HBr photolysis at 243 nm (vertically polarized) and detected by [2+1] REMPI. The outer sphere corresponds to the fast channel producing ground-state Br as coproduct, whereas the inner sphere corresponds to the slow channel yielding spin-orbit-excited Br^*. The different anisotropies of both channels are clearly visible.

Another issue of potential concern is the time resolution of the instrument. While a single event produces a signal of ~5 ns (full width at half maximum, FWHM), the detector has a dead time of 20 ns during which no further events can be recorded. For events within 150 ns the signals on the delay-line wires can overlap but may still be distinguished based on their time sums.[37] The robustness of this technique could not be tested in the present studies because the probability of two events occurring within 150 ns was negligible for the low count rates (typically 0.2 events/laser shot) used. Specifically, the output of the photolysis laser was restricted ($E \leqslant 0.3$ mJ/pulse) to avoid nonresonant ionization of H or D atoms, which meant that the probe laser had to be operated at an even lower power ($E \approx 50\ \mu$J/pulse) to limit its unwanted contribution to photolysis.

IV. VELOCITY CALIBRATION

A. HBr and DBr photolysis

Measurement of the velocity distribution for a well-known system is needed for calibration of the instrument and can serve as a stringent test for its performance. Most importantly, the speed of the test system must be known with high precision to provide a reliable absolute reference for the calibration. Also, very narrow speed distributions are desirable for determining the speed resolution of the instrument.

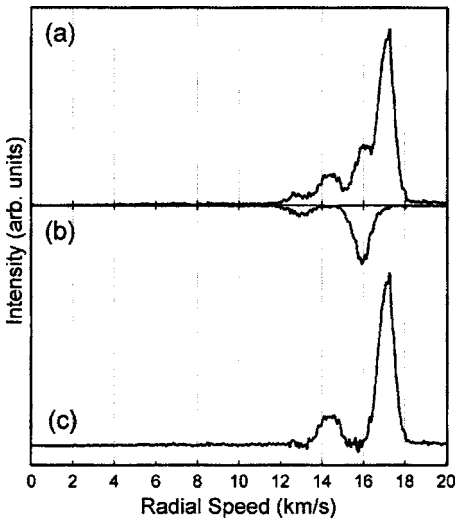

FIG. 5. Radial speed distributions of H atoms (a) formed upon HBr photolysis at 233 nm with contaminating contributions from probe-laser photolysis, (b) from photolysis by the probe laser only, and (c) exclusively from 233 nm HBr photolysis as derived by subtraction of (b) from (a).

H and D atoms produced by laser photolysis of HBr and DBr, respectively, meet these requirements. The bond dissociation energy of HBr is well known $[D_0(\mathrm{H-Br}) = 3.758 \pm 0.003$ eV$]$,[38] and by variation of the wavelength of the photolysis light, different speeds $v(\mathrm{H})$ can be conveniently accessed. These speeds are sharp because no energy can be stored in vibrational or rotational modes of the atomic photoproducts. However, electronic excitation may occur for Br:

$$\mathrm{HBr} + h\nu \rightarrow \mathrm{H} + \mathrm{Br}(^2P_{3/2}) \tag{4a}$$

$$\rightarrow \mathrm{H} + \mathrm{Br}^*(^2P_{1/2}). \tag{4b}$$

In the case of spin-orbit excitation, Eq. (4b), $\Delta E_{\mathrm{SO}} = 0.457$ eV (Ref. 31) is no longer available for acceleration of the H atom. Therefore, we refer to Eq. (4b) as the slow channel, in contrast to the fast channel, which yields ground-state Br, Eq. (4a). This nomenclature becomes immediately clear from inspection of Fig. 4.

The slow channel provides additional data points, but also complicates the analysis because of overlapping speed distributions. Operating at 243 nm for [2+1] REMPI of atomic hydrogen, the probe laser can photolyze HBr as well and thus produces H atoms moving more slowly than H atoms from independent photolysis at shorter wavelengths. The slow channel of the latter can overlap with the fast channel of the former. To resolve this interference, the signal stemming from photolysis by the probe laser is recorded by appropriately delaying the photolysis laser pulse on an every-other-shot basis (normally, the photolysis pulse precedes the probe pulse by about 2 ns); subtraction then yields the uncontaminated speed distribution for the H atoms formed by the independent photolysis laser (Fig. 5). Usually, at least 10 000 events (corresponding to $\geqslant$2 h collection time) were required to obtain images of sufficient quality for extracting reliable speed and angular distributions. We anticipate that similar times would be required for imaging angular distributions from bimolecular reactions.

B. Doppler-free spectroscopy

Because of their high speeds, H and D atoms from HBr and DBr photolysis show substantial Doppler shifts in their [2+1] REMPI spectra. Although it is possible to record the complete 3D velocity distribution by scanning the wavelength domain, this approach is susceptible to power fluctuations of the probe laser and inefficient because only a small fraction of the H atoms can be resonantly ionized at a given wavelength. To exclude these potential problems, we employ Doppler-free spectroscopy for all [2+1] REMPI calibration measurements (see Sec. II B).[39] Doppler-free spectroscopy ionizes H atoms irrespective of their speed in the direction of the laser propagation, thereby strongly increasing the signal without affecting the background. Enhanced signal-to-background ratios are particularly important for studying systems with inherently small signals, such as bimolecular reactions. While Doppler-free spectroscopy has been applied in 2D ion imaging,[40] it has not been previously used for 3D ion imaging with a delay-line detector.

C. Absolute speeds

As shown above, a linear relation exists between the differential time signals from the delay-line anode, $\Delta\tau_x$ and $\Delta\tau_y$, and the x and y coordinates of the ion's position of arrival at the detector. Because no electrostatic fields are present in the xy plane, the ions move with constant speeds v_x and v_y, which are thus immediately derived from Eq. (1) as

$$v_x = s_x \cdot \Delta\tau_x/\tau \tag{5a}$$

and

$$v_y = s_y \cdot \Delta\tau_y/\tau. \tag{5b}$$

Combination with Eq. (3) allows calculation of the overall radial speed v_{exp} as follows:

$$v_{\mathrm{exp}} = [v_x^2 + v_y^2 + v_z^2]^{1/2} = [(s_x^2\Delta\tau_x^2 + s_y^2\Delta\tau_y^2)/\tau^2 + c_z^2\Delta\tau^2]^{1/2}. \tag{6}$$

We then adjust the calibration parameters s_x, s_y, and c_z until the deviation between $v_{\mathrm{exp}}(\mathrm{D}, \lambda_{\mathrm{photolysis}} = 243$ nm) and the calculated, exact speed $v_{\mathrm{cal}}(\mathrm{D}, \lambda_{\mathrm{photolysis}} = 243$ nm) is minimized. We base the calibration on the 243 nm photolysis data because for this wavelength one laser can be used both for photodissociation and REMPI, which facilitates the experiment and also renders background subtraction unnecessary. Furthermore, we choose DBr instead of HBr photolysis to avoid any potential bias in favor of high speeds, since future applications will involve the measurement of slower HD molecules. In addition, the speed distributions for the D atoms are slightly narrower than for the H atoms (see Sec. IV D). A comparison of the final values obtained for v_{exp} with v_{cal} shows favorable agreement both for DBr and HBr photolysis for all wavelengths studied and thus proves good reliability of the calibration (Fig. 6). Also note that the TOF

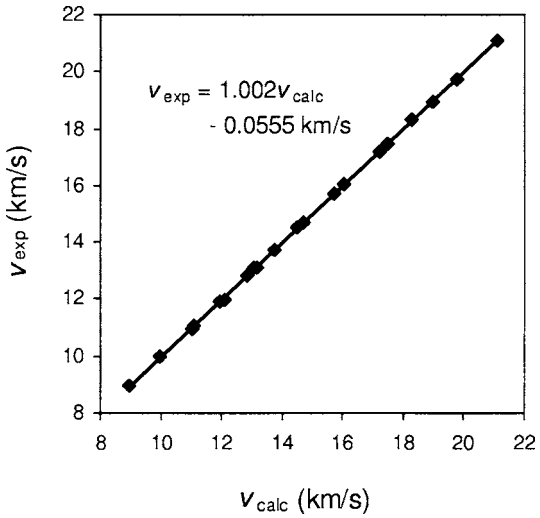

FIG. 6. Correlation between measured speeds ν_{exp} and calculated speeds ν_{calc}.

voltages were adjusted in each experiment to match the spread of the ions to the diameter of the detector. The observed close correlation between ν_{exp} and ν_{cal} demonstrates that the calibration factors derived are independent of the TOF voltages. Our ability to determine accurate speeds over a large range (average error 0.3%, maximum error 1.0%) suggests that the instrument is well suited for the measurement of velocity distributions.

D. Speed resolution

Another important criterion for the performance of the instrument is the achieved speed resolution. For the fast channel, the measured speed distributions of H atoms show widths (FWHM) of about 900 m s^{-1}, which corresponds to relative resolutions of ~5%. A significant contribution to this broadening results from the recoil that the expelled electron imparts on the H^+ cation in the [2+1] REMPI process, ν_{rec}=420 m s^{-1}. For the heavier D^+, the calculated recoil speed is smaller (ν_{rec}=210 m s^{-1}), and indeed we find a slightly better relative resolution for DBr photolysis (~4.5% for the fast channel). To determine our instrumental resolution without the limiting effect of ionization recoil, we also studied speed distributions of H atoms with [3+1] REMPI,

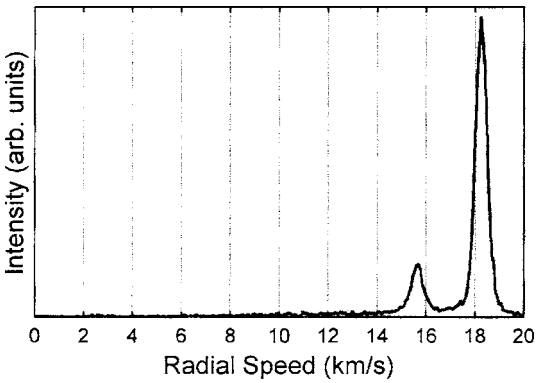

FIG. 7. Radial speed distribution of H atoms formed upon HBr photolysis at 225 nm and detected by [3+1] REMPI.

which deposits hardly any energy into the atom in excess of the ionization threshold (ν_{rec}=20 m s^{-1});[41,42] alternatively, the broadening by the ionization recoil could be overcome by numerical deconvolution.[14] For photolysis at 225 nm, we found a distribution with a width of 630 m s^{-1} and a relative resolution of 3.4%. As a comparison of Figs. 5 and 7 shows, this result represents a significant improvement over the [2+1] REMPI experiment. Our resolution can also be compared with the results of Chichinin *et al.*[22] for the speed of atomic chlorine produced from Cl_2 photolysis as measured with their delay-line instrument. These authors achieve an absolute speed resolution of ~200 m s^{-1}, corresponding to a relative resolution of >10%.

The remaining finite width of the measured speed distributions points to the presence of other blurring sources. The Gaussian profiles of the observed distributions exhibit relative broadening in x and y in accord with the expected Gaussian-shaped focal volume of the probe laser (only its finite extension in the xy plane matters because of space focusing in the z direction, see Sec. III B). Additional contributions to the broadening arise from imperfect cooling in the molecular beam, the finite widths of the laser pulses and of the MCP signal, and time jitter of the laser Q switches and the discriminator. Note that the presence of two bromine isotopes in HBr scarcely contributes to velocity broadening ($\Delta\nu \leqslant 5$ m s^{-1}).

TABLE I. Fraction of slow channel Γ[a], H-atom speeds, and anisotropy parameters as functions of HBr photolysis conditions.

	Fraction of slow channel I[a]		Fast channel (Formation of ground-state Br)					Slow channel (Formation of excited Br*)				
						Anisotropy					Anisotropy	
$\lambda_{photolysis}$ (nm)	Γ_{exp}	Γ_{lit}[b]	ν_{exp}(H) (m s^{-1})	ν_{calc}(H)[c] (m s^{-1})	$\Delta\nu$(H)/ ν_{calc}(H) (%)	β_{exp}	β_{lit}[b]	ν_{exp}(H) (m s^{-1})	ν_{calc}(H)[c] (m s^{-1})	$\Delta\nu$(H)/ ν_{calc}(H) (%)	β_{exp}	β_{lit}[b]
203.29	0.17±0.03	0.16±0.03	21 110	21 110	0.0	−1.0±0.1	$-1.0^{+0.4}_{-0.0}$	18 930	18 953	−0.1	0.2±0.3	$0.6^{+0.4}_{-0.5}$
213.31	0.18±0.04	0.17±0.03	19 760	19 784	−0.1	−0.9±0.1	$-1.0^{+0.4}_{-0.0}$	17 440	17 465	−0.1	0.9±0.3	$1.0^{+0.7}_{-0.4}$
225.01	0.18±0.02	0.18±0.03	18 310	18 284	0.1	−1.0±0.1	$-1.0^{+0.4}_{-0.0}$	15 700	15 745	−0.3	1.3±0.2	$1.5^{+0.5}_{-0.4}$
233.36	0.18±0.03	0.22±0.03	17 180	17 234	−0.3	−0.9±0.1	$-1.0^{+0.4}_{-0.0}$	14 490	14 512	−0.2	1.6±0.3	$1.7^{+0.3}_{-0.3}$
243.13	0.20±0.02	0.17±0.03	16 040	16 019	0.1	−1.0±0.1	$-1.0^{+0.4}_{-0.0}$	13 090	13 047	0.3	1.5±0.3	$2.0^{+0.0}_{-0.7}$

[a]Defined as $[Br^*]/([Br]+[Br^*])$.
[b]Interpolation of data points reported in Ref. 28.
[c]Calculated under inclusion of E_{rot}(HBr).

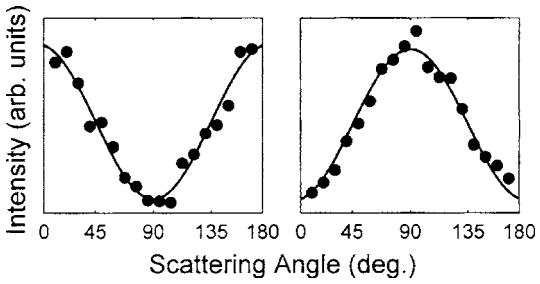

FIG. 8. Experimental angular distributions of H atoms from the slow (left) and fast (right) channels of HBr photolysis at 233 nm with fits (β=1.6±0.3 and −0.9±0.1). The distributions shown are corrected for contamination from photolysis by the probe laser.

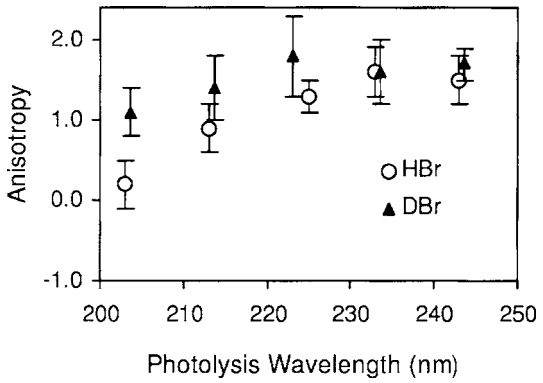

FIG. 9. Anisotropies of the slow channel for HBr and DBr photolysis as functions of wavelength.

V. MEASUREMENT OF BRANCHING RATIOS AND ANISOTROPIES

In addition to the derivation of speed distributions, we can also determine the branching ratio between the fast and slow channels and the angular distribution of H and D photofragments. For one-photon dissociation of HBr with linearly polarized light, the angular distribution of H atoms is given as

$$f(\alpha) = 1 + \beta \cdot P_2(\alpha) = 1 + \beta \cdot (3\cos^2\alpha - 1)/2, \qquad (7)$$

where α is the angle between the vector of the electric field of the photolysis light and the velocity of the H atoms, β is the anisotropy, and P_2 the second Legendre polynomial.[43] The two limiting cases, $\beta=-1$ and $\beta=2$, correspond to perpendicular $[f(\alpha)\sim\sin^2\alpha]$ and parallel $[f(\alpha)\sim\cos^2\alpha]$ angular distributions, as exemplified by the fast and slow channels of HBr photolysis at $\lambda=243$ nm (Fig. 4).

We compare our results to the findings of Regan *et al.*,[28] who also studied the dependence of HBr photolysis on wavelength. The branching fractions we determined agree with those reported by Regan *et al.* within the experimental uncertainties (Table I). In our experiment, the branching fraction is a sensitive probe for the extent to which Doppler-free conditions are achieved. For imperfect conditions and significant contributions of Doppler-shifted signal, resonant ionization preferentially occurs for H atoms with slow speeds parallel to the propagation of the probe laser. In the present geometry, this corresponds to a potential bias toward the slow channel with its angular distribution parallel to the z direction. While some residual Doppler background signal inevitably arises from H atoms traveling with zero velocity along the propagation direction of the probe laser,[39] the absence of a significant bias in our experiment demonstrates that these contributions were negligibly small.

Anisotropy parameters were determined by fitting the measured angular distributions after subtraction of contaminating contributions from photolysis by the probe laser (Fig. 8). To avoid potential interference by residual Doppler signal, H and D atoms scattered along the z axis ($\alpha<9°$ or $\alpha>171°$) were excluded in this analysis. The fact that Eq. (7) without the inclusion of higher Legendre moments successfully describes the measured angular distributions rules out the possibility of unwanted alignment of HBr in the molecular beam. Whereas the fast channel yields a perpendicular distribution for all wavelengths studied, the anisotropy of the slow channel changes markedly (Table I). These observations match the results of Regan *et al.*[28] and thus, once again, indicate proper functioning of the instrument. In particular, correction for the contamination from probe-laser photolysis by subtraction of the corresponding signal works well.

To the best of our knowledge, the wavelength dependence of DBr photolysis has not been studied previously. We find that the fraction of spin-orbit-excited Br^* is slightly, but consistently, lower than for HBr photolysis (Table II). While the anisotropy of the fast channel is the same as for HBr photolysis, that of the slow channel differs for the shorter wavelengths sampled (Table II and Fig. 9).

These isotope effects might reflect altered Franck-Condon factors. The larger zero-point energy of HBr leads to a Franck-Condon region shifted to slightly higher energies

TABLE II. Fraction of slow channel, D-atom speeds, and anisotropy parameters as functions of DBr photolysis conditions.

		Fast channel (Formation of ground-state Br)				Slow channel (Formation of excited Br^*)			
$\lambda_{photolysis}$ (nm)	Fraction of slow channel Γ[a]	v_{exp}(D) (m s^{-1})	v_{calc}(D)[b] (m s^{-1})	Δv(D)/v_{calc}(D) (%)	Anisotropy β	v_{exp}(D) (m s^{-1})	v_{calc}(D)[b] (m s^{-1})	Δv(D)/v_{calc}(D) (%)	Anisotropy β
203.29	0.13±0.02	14 690	14 699	−0.1	−0.9±0.1	13 080	13 167	−0.7	1.1±0.3
213.31	0.14±0.03	13 720	13 758	−0.3	−1.0±0.2	11 990	12 107	−1.0	1.4±0.4
223.34	0.14±0.02	12 790	12 841	−0.4	−1.0±0.1	10 960	11 054	−0.9	1.8±0.5
233.36	0.14±0.03	11 920	11 942	−0.2	−1.0±0.1	9 990	9 996	−0.1	1.6±0.4
243.07	0.14±0.02	11 080	11 081	0.0	−1.0±0.1	8 970	8 949	0.2	1.7±0.2

[a]Defined as $[Br^*]/([Br]+[Br^*])$.
[b]Calculated under inclusion of E_{rot}(DBr).

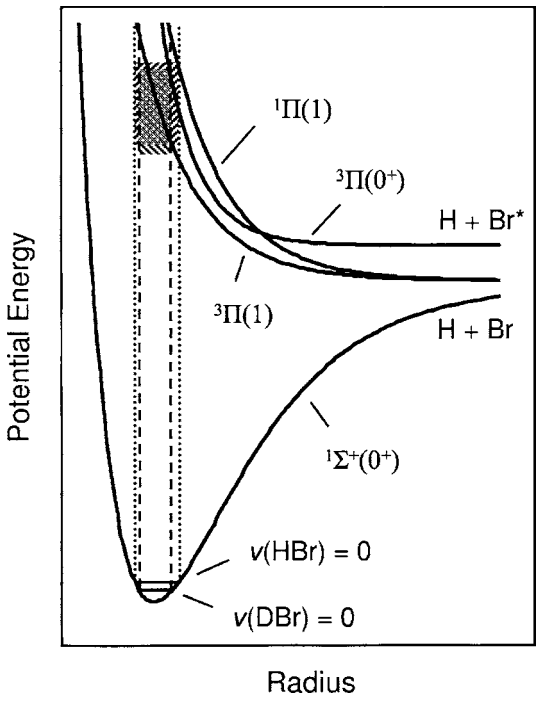

FIG. 10. Schematic potential energy diagram for HBr/DBr with the classically allowed Franck-Condon regions (hatched) relevant to the present study.

and extended to slightly longer internuclear distances in comparison with DBr (Fig. 10). For the photolysis wavelengths sampled in the present study, this shift of the classically allowed Franck-Condon region is expected to make transitions to the $^3\Pi(0^+)$ excited state relatively more likely for HBr than for DBr. Because the $^3\Pi(0^+)$ state correlates with spin-orbit-excited bromine in the dissociation limit, Eq. (4b),[28] the photodissociation of HBr is anticipated to favor the slow channel compared to DBr. While this simple argument can rationalize our observations, a more rigorous analysis must also consider the possible involvement of the $^1\Pi(1)$ state and differences in the transition dipole moments.[44,45]

VI. COMPARISON WITH OTHER METHODS

The present instrument is considerably more complex and expensive than the previous apparatus used in our laboratory for the determination of speed distributions by the core-extraction method.[8] To justify the increased costs the new instrument should offer significantly enhanced performance. We think that this is the case for the following reasons: (i) The new instrument allows the measurement of 3D velocity distributions and thus yields inherently more information than the 1D core-extraction method; (ii) in contrast to core extraction, the new instrument collects all ions formed, thereby improving the signal-to-background ratio; (iii) the sensitivity of the present 3D detection scheme is velocity independent and thus, unlike core extraction, is not biased against forward-scattered products, which often contain particularly interesting dynamical information;[46–48] and (iv) with the new instrument, we achieve absolute velocity resolutions of about 900 m s^{-1} for [2+1] REMPI and 630 m s^{-1} for [3+1] REMPI of atomic hydrogen, whereas a value of 1700 m s^{-1} is the best resolution reported for the old apparatus ([2+1] REMPI of H atoms from HBr photolysis).[8]

Other recently developed imaging techniques involve instrumentation similarly demanding as the method we described, but differ in important aspects. Both conventional ion imaging and the different variants of sliced ion imaging can tolerate much higher count rates than delay-line detection with its limited multihit resolution. In sliced ion imaging, this potential advantage is somewhat compromised because only the central slice of the whole 3D sphere of ions is collected. Nevertheless, the possibility of velocity focusing allows for impressive velocity resolutions for this technique. For [3+1] REMPI of atomic hydrogen formed upon HBr photolysis, relative resolutions of 0.5% and 1.5% have been recently achieved,[41,42] which are superior to the 3.4% we obtain with our instrument. However, sliced ion imaging cannot measure the entire 3D velocity distribution and also exhibits a velocity-dependent sensitivity. Conventional ion imaging, in turn, yields complete 3D velocity distributions, but only through numerical inversion techniques that impose symmetry restrictions and are prone to amplify noise and introduce artifacts. In contrast, our experiment directly measures 3D images without the need for complicated analyses.

The different imaging techniques discussed each have their own specific advantages and cannot be rated on an absolute scale because different applications have different requirements. The use of a delay-line anode appears particularly appropriate for studying systems with low signal intensities, such as the $H+D_2$ exchange with its very small reaction cross sections for specific product quantum states. For accurate measurements, the exclusion of detrimental space-charge effects and collisional relaxation is essential and necessarily leads to very low count rates.[8] The determination of differential cross sections for the $H+D_2$ exchange reaction will be the main objective of future applications of the new instrument.

VII. CONCLUSIONS

We describe a new instrument that combines Doppler-free REMPI with 3D delay-line detection. The apparatus shows promising characteristics for the determination of 3D velocity distributions of products from photoinitiated reactions. From the analysis of speed distributions of H and D atoms from HBr and DBr photolysis, respectively, we derive an average error of ±0.3% for the measured radial speed and a relative resolution of 3.4%. To achieve this resolution, [3+1] instead of [2+1] REMPI is necessary to overcome velocity broadening from the recoil of the emitted photoelectron. In addition, our measurements correctly reproduce the branching between ground-state and spin-orbit-excited product channels as well as the anisotropies of HBr photolysis reported in the literature. We provide analogous results for DBr photolysis, which received little attention previously. These data may prove useful for rigorous quantitative analysis of bimolecular reactions involving D atoms as reactants.

The delay-line detector described has favorable characteristics for recording single ions and measuring their 3D velocity, but is limited to rather low count rates because of its

finite multihit resolution and also because of its sensitivity to stray UV light. Therefore, its prime application should be the investigation of bimolecular reactions, which usually yield only low signal levels for a specific product quantum state.

ACKNOWLEDGMENTS

The authors thank O. Jagutzki and A. Czasch, RoentDek Handels GmbH (Kelkheim, Germany), for assistance with the implementation of the delay-line anode and J. P. Camden, D. J. A. Brown, M. R. Martin, and I. Zuleta for helpful discussions and valuable advice. One of the authors (K.K.) thanks the Deutsche Forschungsgemeinschaft for an Emmy Noether fellowship (KO 2875/1-1). Support by the National Science Foundation under Grant No. NSF CHE 0242103 is gratefully acknowledged.

[1] R. D. Levine, *Molecular Reaction Dynamics* (Cambridge University Press, Cambridge, UK, 2005).
[2] Y. T. Lee, J. D. McDonald, P. R. LeBreton, and D. R. Herschbach, Rev. Sci. Instrum. **40**, 1402 (1969).
[3] Y. T. Lee, Angew. Chem. **99**, 967 (1987); Angew. Chem., Int. Ed. Engl. **26**, 939 (1987).
[4] D. R. Herschbach, Angew. Chem. **99**, 1251 (1987); Angew. Chem., Int. Ed. Engl. **26**, 1221 (1987).
[5] N. E. Shafer, A. J. Orr-Ewing, W. R. Simpson, H. Xu, and R. N. Zare, Chem. Phys. Lett. **212**, 155 (1993).
[6] N. E. Shafer-Ray, A. J. Orr-Ewing, and R. N. Zare, J. Phys. Chem. **99**, 7591 (1995).
[7] W. R. Simpson, A. J. Orr-Ewing, T. P. Rakitzis, S. A. Kandel, and R. N. Zare, J. Chem. Phys. **103**, 7299 (1995).
[8] F. Fernández-Alonso, B. D. Bean, and R. N. Zare, J. Chem. Phys. **111**, 1022 (1999).
[9] D. W. Chandler and P. L. Houston, J. Chem. Phys. **87**, 1445 (1987).
[10] A. T. J. B. Eppink and D. H. Parker, Rev. Sci. Instrum. **68**, 3477 (1997).
[11] M. J. J. Vrakking, Rev. Sci. Instrum. **72**, 4084 (2001).
[12] K. Zhao, T. Colvin, W. T. Hill III, and G. Zhang, Rev. Sci. Instrum. **73**, 3044 (2002).
[13] M. J. Bass, M. Brouard, A. P. Clark, and C. Vallance, J. Chem. Phys. **117**, 8723 (2002).
[14] F. Renth, J. Riedel, and F. Temps, Rev. Sci. Instrum. **77**, 033103 (2006).
[15] C. R. Gebhardt, T. P. Rakitzis, P. C. Samartzis, V. Ladopoulos, and T. N. Kitsopoulos, Rev. Sci. Instrum. **72**, 3848 (2001).
[16] J. J. Lin, J. Zhou, W. Shiu, and K. Liu, Rev. Sci. Instrum. **74**, 2495 (2003).
[17] D. Townsend, M. P. Minitti, and A. G. Suits, Rev. Sci. Instrum. **74**, 2530 (2003).
[18] D. A. Chestakov, S. M. Wu, G. R. Wu, D. H. Parker, A. T. J. B. Eppink, and T. N. Kitsopoulos, J. Phys. Chem. A **108**, 8100 (2004).
[19] M. Lampton, O. Siegmund, and R. Raffanti, Rev. Sci. Instrum. **58**, 2298 (1987).
[20] J. Ullrich, R. Moshammer, R. Dörner, O. Jagutzki, V. Mergel, H. Schmidt-Böcking, and L. Spielberger, J. Phys. B **30**, 2917 (1997).
[21] J. A. Davies, J. E. LeClaire, R. E. Continetti, and C. C. Hayden, J. Chem. Phys. **111**, 1 (1999).
[22] A. I. Chichinin, T. Einfeld, C. Maul, and K.-H. Gericke, Rev. Sci. Instrum. **73**, 1856 (2002).
[23] A. Czasch, L. P. H. Schmidt, T. Jahnke, T. Weber, O. Jagutzki, S. Schössler, M. S. Schöffler, R. Dörner, and H. Schmidt-Böcking, Phys. Lett. A **347**, 95 (2005).
[24] A. S. Alnaser, C. M. Maharjan, X. M. Tong, B. Ulrich, P. Ranitovic, B. Shan, Z. Chang, C. D. Lin, C. L. Cocke, and I. V. Litvinyuk, Phys. Rev. A **71**, 031403(R) (2005).
[25] O. Geßner, A. M. D. Lee, J. P. Shaffer *et al.*, Science **311**, 219 (2006).
[26] Z. Xu, B. Koplitz, and C. Wittig, J. Phys. Chem. **92**, 5518 (1988).
[27] T. Kinugawa and T. Arikawa, J. Phys. Chem. **96**, 4801 (1992).
[28] P. M. Regan, S. R. Langford, A. J. Orr-Ewing, and M. N. R. Ashfold, J. Chem. Phys. **110**, 281 (1999).
[29] R. Baumfalk, U. Buck, C. Frischkorn, N. H. Nahler, and L. Hüwel, J. Chem. Phys. **111**, 2595 (1999).
[30] E. E. Marinero, C. T. Rettner, and R. N. Zare, Phys. Rev. Lett. **48**, 1323 (1982).
[31] C. E. Moore, *Atomic Energy Levels*, Natl. Bur. Stand. (U.S.) Circ. No. 467 (U.S. GPO, Washington, D.C. 1971), Vol. 1; Natl. Bur. Stand. (U.S.) Circ. No. 467 (U.S. GPO, Washington, D.C., 1971), Vol. 2.
[32] R. Callaghan and R. J. Gordon, J. Chem. Phys. **93**, 4624 (1990).
[33] L. R. Brewer, F. Buchinger, M. Ligare, and D. E. Kelleher, Phys. Rev. A **39**, 3912 (1989).
[34] W. C. Wiley and L. H. McLaren, Rev. Sci. Instrum. **26**, 1150 (1955).
[35] D. A. Dahl, SIMION 3D, Version 6.0, U.S. Department of Energy, Office of Energy Research, Idaho Falls, ID, 1995.
[36] E. Liénard, M. Herbane, G. Ban *et al.*, Nucl. Instrum. Methods Phys. Res. A **551**, 375 (2005).
[37] O. Jagutzki, V. Mergel, K. Ullmann-Pfleger, L. Spielberger, U. Spillmann, R. Dörner, and H. Schmidt-Böcking, Nucl. Instrum. Methods Phys. Res. A **477**, 244 (2002).
[38] M. W. Chase, Jr., J. Phys. Chem. Ref. Data Monogr. **9**, 429 (1998).
[39] A. E. Pomerantz and R. N. Zare, Chem. Phys. Lett. **370**, 515 (2003).
[40] J. Riedel, S. Dziarzhytski, A. Kuczmann, F. Renth, and F. Temps, Chem. Phys. Lett. **414**, 473 (2005).
[41] R. L. Toomes, P. C. Samartzis, T. P. Rakitzis, and T. N. Kitsopoulos, Chem. Phys. **301**, 209 (2004).
[42] W. Li, S. D. Chambreau, S. A. Lahankar, and A. G. Suits, Rev. Sci. Instrum. **76**, 063106 (2005).
[43] R. N. Zare, Mol. Photochem. **4**, 1 (1972).
[44] J. P. Camden, H. A. Bechtel, D. J. A. Brown, A. E. Pomerantz, R. N. Zare, and J. R. Le Roy, J. Phys. Chem. A **108**, 7806 (2004).
[45] D. A. Chapman, K. Balasubramanian, and S. H. Lin, Chem. Phys. **118**, 333 (1987).
[46] D. A. Neumark, A. N. Wodtke, G. N. Robinson, C. C. Hayden, and Y. T. Lee, Phys. Rev. Lett. **53**, 226 (1984).
[47] F. Fernández-Alonso, B. D. Bean, J. D. Ayers, A. E. Pomerantz, R. N. Zare, L. Bañares, and F. J. Aoiz, Angew. Chem. **112**, 2860 (2000); Angew. Chem., Int. Ed. **39**, 2784 (2000).
[48] M. Qiu, Z. Ren, L. Che *et al.*, Science **311**, 1440 (2006).